DOI 10.15622/sp.2020.19.3.4

N. AL -HEMEARY, P. POLCZ, G. SZEDERKÉNYI

OPTIMAL SOLAR PANEL AREA COMPUTATION AND TEMPERATURE TRACKING FOR A CUBESAT SYSTEM USING MODEL PREDICTIVE CONTROL

Al-Hemeary N., Polcz P., Szederkényi G. **Optimal Solar Panel Area Computation and Temperature Tracking for a CubeSat System using Model Predictive Control.**

Abstract. Recently, there has been a rising interest in small satellites such as CubeSats in the aerospace community due to their small size and cost-effective operation. It is challenging to ensure precision performance for satellites with minimum cost and energy consumption. To support maneuverability, the CubeSat is equipped with a propellant tank, in which the fuel must be maintained in the appropriate temperature range. Simultaneously, the energy production should be maximized, such that the other components of the satellite are not overheated. To meet the technological requirements, we propose a multicriteria optimal control design using a nonlinear dynamical thermal model of the CubeSat system. First, a PID control scheme with an anti-windup compensation is employed to evaluate the minimum heat flux necessary to keep the propellant tank at a given reference temperature. Secondly, a linearization-based controller is designed for temperature control. Thirdly, the optimization of the solar cell area and constrained temperature control is solved as an integrated nonlinear model predictive control problem using the quasi-linear parameter varying form of the state equations. Several simulation scenarios for different power limits and solar cell coverage cases are shown to illustrate the trade-offs in control design and to show the applicability of the approach.

Keywords: Aerospace Systems, CubeSat, Nonlinear MPC, Actuator Power, Nonlinear Dynamical Model, Feedback Linearization.

1. Introduction.

The increase of interest toward cube-shaped miniaturized satellites (CubeSats) has grown rapidly in the space community including space agencies, industry, and academic research due to the low cost of a CubeSat mission. The mass of a CubeSat is approximately 1 kilogram with all dimensions being 10 centimeters long as specified by California State Polytechnic, and the Space Systems Design Lab (SSDL) at the Georgia Institute of Technology as the innovators of this satellite technology [1]. The CubeSat electronics equipment is energized by a small battery, which recharges via solar panels mounted on the satellite surface. However, the power generated by solar panels is always a significant concern because of the small surface of CubeSats.

So far, a limited number of CubeSats have used thrust systems for orbital maneuvers such as drags recovery or flight formation. As the CubeSat mission capabilities are of great interest, many propulsion systems such as electric, chemical or cold gas-based propulsion systems, and solar sails have been introduced for CubeSats maneuvers [2,3]. To investigate the thermal conditions of installing a fuel tank inside a CubeSat, a thermal dynamical model was

derived and simulated in [4], where the thermal fluctuation effect caused by the sunlight during the orbital motion was modeled as a time-varying disturbance signal. Due to the low power consumption requirements, the thermal control problem of a CubeSat is challenging during the satellite orbits. Therefore, a passive control system was proposed also in [4] to maintain the temperature of the fuel tank close to the desired thermal limits.

In order to obtain an optimal tracking performance of the propellant tank temperature, an active control system has to be applied. A simple PID controller was proposed in [5] to eliminate the thermal fluctuation of the propellant tank temperature within the CubeSat orbit. In [6], a nonlinear feedback law based on input-output linearization was described to maintain the fuel tank on the prescribed temperature.

In the last decades, the Linear Parameter Varying (LPV) paradigm has drawn much attention and become a standard formalism in systems and control theory. An LPV framework treats linear dynamical systems that have state-space representations depending on time-varying parameters, thus it can be considered as the natural extension of the linear time-invariant (LTI) framework [9, 10]. Furthermore, the LPV framework is a popular approach to rewrite nonlinear systems by involving nonlinearities in the scheduling parameters, and in this way, it is possible to extend some of the linear control techniques for nonlinear systems [11]. The combination of LPV control and feedback linearization has been implemented in [12] to provide a general control method of input-affine nonlinear systems. Nevertheless, instead of linearizing the nonlinear systems, set-valued methods with quasi-Linear Parameter Varying (quasi-LPV) representations have been developed for nonlinear systems [13]. The LPV models can be employed to describe nonlinear models derived by nonlinear differential equations that are concerned with physical relations. Often a nonlinear state-space model can be embedded into the so-called quasi-LPV model class [14–16], in which the time-varying parameters are typically disturbance signals or functions of the state, input, and/or output. In [17], three different quasi-LPV model formulation techniques are discussed, namely, state transformation, function substitution, and an LPV extension for the well-known Jacobian (linear approximation) method.

Due to the rapid growth of computational power in the last few decades, a new control methodology emerged in the systems and control community based on prediction and optimization. These concepts are collectively called as the *model predictive control* (MPC) framework, which spans a fairly wide class of system models. Many results are available for general nonlinear systems, for example, in [16, 17]. Other MPC techniques are formulated specifically for nonlinear models in a quasi-LPV form, see e.g. [18–22]. Several useful

numerical techniques of [16, 17, 23–26] were implemented in MATLAB's Model Predictive Control Toolbox [27].

These new theoretical/computational results provide new possibilities to manufacture and operate CubeSats to meet the technological thermal constraints. It is challenging that the thermal controller design has multiple objectives. Firstly, we have to keep *propellant tank on approximately room temperature* with minimal or no fluctuation. The temperature of the CubeSat's surface should not exceed a given upper bound. Secondly, a control signal has to be computed which can be realized with the on-board heater, namely, it must be non-negative and *not exceed an upper power limit*. On the other hand, we are interested in *maximizing the area* of the solar panel to produce more electrical energy to operate the on-board computer or other (e.g., telecommunication) devices or sensors. It is worth mentioning that the solar panel significantly influences the average/baseline temperature level of each component of the CubeSat object. Therefore, the proportion (λ) of the solar panel area ($A_{\mathrm{P}} = \lambda A_{\mathrm{F}}$) and the total face area (A_{F}) are distinguished design parameters in the manufacturing of the CubeSat.

In an earlier phase of this research [28], we fixed λ to a low value ($\lambda = 0.3$) and designed a PID control loop with different actuator power limits. Furthermore, a linearization method was employed to regulate temperature levels. In this paper, we extend the results of [28], with the integrated design of an *optimal* solar panel area and an appropriate control signal, which together provide that the component temperatures fulfill the prescribed technological constraints.

The paper is organized as follows: A brief mathematical model description of the CubeSat's dynamical thermal behavior and its possible quasi-LPV model formulation is presented in Section 2. Preliminary research results of [28] are summarized for comparison in Sections 3 and 4. Finally, an integrated model predictive control design approach is presented in Section 5.

2. CubeSat surface and propellant tank thermal mathematical model. The thermal mathematical model of the CubeSat surface and its propellant tank has been developed assuming that the CubeSat has a circular orbital motion of 1.5 hours ($P = 5400\,\mathrm{s}$ orbital period), which is divided into three parts (intervals). In the first part P_1 of its orbital period, the CubeSat spends a quartile of its orbital time in the presence of sunlight (first luminous part). In the second part P_2, the CubeSat spends half of its orbital time in the shadow of the Earth (eclipse part). In the third part P_3, the satellite orbits again in the sight of the Sun (second luminous part).

In [4, 5], a mathematical model is given for the thermal behaviour of the satellite's surface and tank (separately for each orbital interval P_1, P_2 and P_3) in the form of nonlinear *switched* ordinary differential equations . In this

paper, we consider the governing equations of the CubeSat's thermal dynamics in an *equivalent* "unified" state-space model formulation as follows:

$$
\begin{aligned}
k_{\text{Al-sc}}(\lambda)\,\dot{T}_1 &= \dot{Q} + \dot{Q}_{\text{F}_1} + G_s\,a_{s,\text{Al-sc}}(\lambda)\,A_{\text{F}}\,\rho_1(t) - \\
&\quad - \varepsilon_{\text{IR,Al-sc}}(\lambda)\,\sigma\,A_{\text{F}}\,T_1^4, \\
k_{\text{Al-sc}}(\lambda)\,\dot{T}_2 &= \dot{Q} + \dot{Q}_{\text{F}_2} + G_s\,a_{s,\text{Al-sc}}(\lambda)\,A_{\text{F}}\,\rho_2(t) - \\
&\quad - \varepsilon_{\text{IR,Al-sc}}(\lambda)\,\sigma\,A_{\text{F}}\,T_2^4, \\
k_{\text{Al}}\,\dot{T}_3 &= \dot{Q} + \dot{Q}_{\text{F}_3} + p_{\text{Af}}\,G_s\,a_{s,\text{Al}}\,A_{\text{F}}\,\varrho_1(t) - \\
&\quad - \varepsilon_{\text{IR,Al}}\,\sigma\,A_{\text{F}}\,T_3^4 + a_{\text{IR,Al}}\,\sigma\,A_{\text{F}}\,T_{\text{E}}^4, \\
k_{\text{Al-sc}}(\lambda)\,\dot{T}_4 &= \dot{Q} + \dot{Q}_{\text{F}_4} + G_s\,a_{s,\text{Al-sc}}(\lambda)\,A_{\text{F}}\,\rho_4(t) - \\
&\quad - \varepsilon_{\text{IR,Al-sc}}(\lambda)\,\sigma\,A_{\text{F}}\,T_4^4, \\
k_{\text{Al}}\,\dot{T}_5 &= \dot{Q} + \dot{Q}_{\text{F}_5} - \varepsilon_{\text{IR,Al}}\,\sigma\,A_{\text{F}}\,T_5^4, \\
k_{\text{Al}}\,\dot{T}_6 &= \dot{Q} + \dot{Q}_{\text{F}_6} - \varepsilon_{\text{IR,Al}}\,\sigma\,A_{\text{F}}\,T_6^4, \\
k_{\text{T}}\,\dot{T}_{\text{T}} &= k_0(T_1^4 + T_2^4 + T_3^4 + T_4^4 + T_5^4 + T_6^4 - 6T_{\text{T}}^4) + \dot{Q}_{\text{c}},
\end{aligned}
\tag{1}
$$

where

$$
\begin{aligned}
&k_{\text{Al}} = m_{\text{Al}}\,c_{p,\text{Al}},\ k_{\text{T}} = m_{\text{s}}\,c_{p,\text{s}} + m_{\text{N}}\,c_{p,\text{N}}\ ,\ k_0 = \theta_{\text{Ft}}\,\varepsilon_{\text{IR,Al}}\,\sigma\,A_{\text{F}}\ , \\
&k_{\text{Al-sc}}(\lambda) = m_{\text{Al}}\,c_{p,\text{Al}} + \lambda\,m_{\text{sc}}\,c_{p,\text{sc}}\ , \\
&a_{s,\text{Al-sc}}(\lambda) = (1-\lambda)\,a_{s,\text{Al}} + \lambda\,a_{s,\text{sc}}\ , \\
&\varepsilon_{\text{IR,Al-sc}}(\lambda) = (1-\lambda)\,\varepsilon_{\text{IR,Al}} + \lambda\,\varepsilon_{\text{IR,sc}}
\end{aligned}
\tag{2}
$$

are auxiliary parameters for more convenient notation. The physical parameters and the time-dependent variables of the model are as follows: $T_{\text{E}} = 255\,\text{K}$ is the Earth's reference temperature, T_{T} [K] is the tank's temperature, $a_{\text{IR,Al}} = 0.09$ is the Aluminum infrared absorptivity, $a_{s,\text{Al}} = 0.09$ is the Aluminum solar absorptivity, $a_{s,\text{sc}} = 0.92$ is the solar cell solar absorptivity, $a_{s,\text{Al-sc}}(\lambda)$ is the Aluminum and solar cell average absorptivity, $\varepsilon_{\text{IR,Al}} = 0.92$ is the Aluminum infrared emissivity, $\varepsilon_{\text{IR,sc}} = 0.85$ is the solar cell infrared emissivity, $\varepsilon_{\text{IR,Al-sc}}(\lambda)$ is the Aluminum and solar cell average infrared emissivity, $\dot{Q}_{\text{c}}$ [W] is the heat flux applied to the tank generated by the heater, $\dot{Q}_{\text{F}_i}$ [W] is the radiated heat transfer between the ith face and the tank, $\dot{Q} = 2\,\text{W}$ is the power dissipated heat rate, $c_{p,\text{Al}} = 980\,\text{J}/(\text{kgK})$ is the specific heat of Aluminum, $c_{p,\text{s}} = 504\,\text{J}/(\text{kgK})$ is the stainless steel specific heat, $c_{p,\text{sc}} = 1600\,\text{J}/(\text{kgK})$ is the solar cell specific heat, $c_{p,\text{N}} = 743\,\text{J}/(\text{kgK})$ is the Nitrogen specific

heat, $m_{\mathrm{Al}} = 0.04\,\mathrm{kg}$ is the mass of an Aluminum face, $m_{\mathrm{N}} = 0.0074\,\mathrm{kg}$ is the mass of nitrogen in the tank, $m_{\mathrm{s}} = 0.0926\,\mathrm{kg}$ is the mass of the tank (stainless steel), $m_{\mathrm{sat}} \simeq 1\,\mathrm{kg}$ is the total mass of CubeSat, $m_{\mathrm{sc}} = 0.0085\,\mathrm{kg}$ is the mass of solar panel covering a whole face, $G_s = 1367\mathrm{W}/\mathrm{m}^2$ is the solar constant, $\sigma = 5.669 \cdot 10^{-8}\,\mathrm{WK}^4/\mathrm{m}^2$ is the Stefan-Boltzmann constant, $A_{\mathrm{F}} = 0.01\,\mathrm{m}^2$ is the area of each face, $p_{\mathrm{Af}} = 0.28$ is the albedo factor, $\theta_{\mathrm{Ft}} = \frac{1}{(1+H)^2}$ is the view factor between a face and the tank, where $H = h/r$, where $h = 0.025\mathrm{m}$ is the distance of the tank's surface to the face, and $r = 0.025\,\mathrm{m}$ is the tank radius.

The radiated heat transfer $\dot{Q}_{\mathrm{F}_i}$ between the ith face and the tank is defined as follows:

$$\dot{Q}_{\mathrm{F}_i} = \theta_{\mathrm{Ft}}\,\varepsilon_{\mathrm{IR,Al}}\,\sigma\,A_{\mathrm{F}}\,(T_{\mathrm{T}}^4 - T_i^4),\ i = 1, \ldots, 6. \tag{3}$$

The tank is equipped with a supplementary heat source (*actuator* or *heater*), which generates the *control signal* $u = \dot{Q}_{\mathrm{c}}$ in the form of a (non-negative) heat flux $\dot{Q}_{\mathrm{c}}$ [9].

Due to sunlight and shadowing effects of the Earth, temperatures of the CubeSat's surface and its fuel tank have typically large fluctuations through the orbit. Functions $\varrho_1, \varrho_2, \varrho_4 : \mathbb{R}_+ \to [-1, 1]$ in (1) are meant to describe this periodic temperature fluctuation phenomenon in the dynamics. These time-varying terms in the dynamics are considered as *known parameter signals* given as follows:

$$\varrho_1(t) = \begin{cases} \cos\left(\frac{2\pi t}{P}\right), & \text{if } \dfrac{2\pi t}{P} \in \left[-\frac{\pi}{2}, \frac{\pi}{2}\right] + 2k\pi,\ k \in \mathbb{Z}, \\ 0, & \text{otherwise}, \end{cases} \tag{4a}$$

$$\varrho_2(t) = \begin{cases} -\sin\left(\frac{2\pi t}{P}\right), & \text{if } \dfrac{2\pi t}{P} \in \left[-\frac{\pi}{2}, 0\right] + 2k\pi,\ k \in \mathbb{Z}, \\ 0, & \text{otherwise}, \end{cases} \tag{4b}$$

$$\varrho_4(t) = \begin{cases} \sin\left(\frac{2\pi t}{P}\right), & \text{if } \dfrac{2\pi t}{P} \in \left[0, \frac{\pi}{2}\right] + 2k\pi,\ k \in \mathbb{Z}, \\ 0, & \text{otherwise}. \end{cases} \tag{4c}$$

Function ϱ_1 has nonzero values only in intervals P_1 and P_3, whereas, functions ϱ_2 and ϱ_4 are nonzero in intervals P_3 and P_1, respectively. The graph of functions ϱ_1, ϱ_2 and ϱ_4 are illustrated in Figure 1.

2.1. Quasi-LPV formulation of the thermal model. Beginning from the nonlinear input-affine dynamical model (1), with seven differential equations formulated with respect to physical laws, an equivalent quasi-LPV model

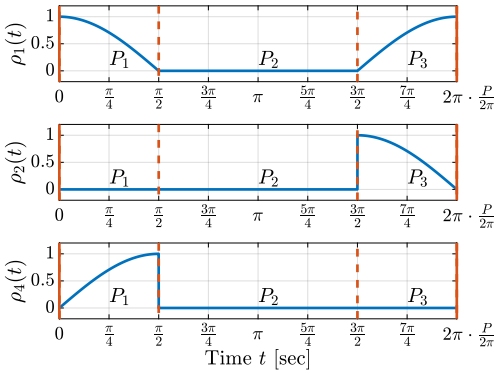

Fig. 1. Graph of functions ρ_1, ρ_2 and ρ_4, which describe the temperature fluctuations of the CubeSat through its the orbital motion

representation can be formulated in the following form:

$$I_k(\lambda)\,\dot{x} = A(x)x + Bu + E(x,\rho)\lambda + F(\rho)\,, \tag{5}$$

where the *state vector* $x = \begin{pmatrix} T_1 & T_2 & T_3 & T_4 & T_5 & T_6 & T_{\mathrm{T}} \end{pmatrix}^{\top} \in \mathbb{R}^n$ ($n = 7$) comprise the six temperature values $(T_1, \ldots, T_6)$ of the six faces of CubeSat, respectively, and the fuel tank's temperature T_{T}. Vector ρ contains the three time-varying parameter signals $\rho = \begin{pmatrix} \rho_1 & \rho_2 & \rho_4 \end{pmatrix}^{\top} \in \mathbb{R}^p$ ($p = 3$), which model the periodic temperature fluctuation effect caused by the sunlight.

Coefficient matrices $I_k(\lambda)$, $A(x)$, B, $E(x,\rho)$ and $F(\rho)$ in (5) are given as follows:

$$I_k(\lambda) = \mathrm{diag}(k_{\text{Al-sc}}(\lambda), k_{\text{Al-sc}}(\lambda), k_{\text{Al}}, k_{\text{Al-sc}}(\lambda), k_{\text{Al}}, k_{\text{Al}}, k_{\mathrm{T}}), \tag{6a}$$

$$A(x) = \begin{pmatrix} -k_{01}T_1^3 & 0 & 0 & 0 & 0 & 0 & k_0 T_{\mathrm{T}}^3 \\ 0 & -k_{01}T_2^3 & 0 & 0 & 0 & 0 & k_0 T_{\mathrm{T}}^3 \\ 0 & 0 & -k_{01}T_4^3 & 0 & 0 & 0 & k_0 T_{\mathrm{T}}^3 \\ 0 & 0 & 0 & -k_{01}T_3^3 & 0 & 0 & k_0 T_{\mathrm{T}}^3 \\ 0 & 0 & 0 & 0 & -k_{01}T_5^3 & 0 & k_0 T_{\mathrm{T}}^3 \\ 0 & 0 & 0 & 0 & 0 & -k_{01}T_6^3 & k_0 T_{\mathrm{T}}^3 \\ k_0 T_1^3 & k_0 T_2^3 & k_0 T_3^3 & k_0 T_4^3 & k_0 T_5^3 & k_0 T_6^3 & -6k_0 T_{\mathrm{T}}^3 \end{pmatrix}, \tag{6b}$$

$$B = \begin{pmatrix} 0 \\ 0 \\ 0 \\ 0 \\ 0 \\ 0 \\ 1 \end{pmatrix}, \; E(x,\rho) = \begin{pmatrix} k_4\varrho_1 - k_2 T_1^4 \\ k_4\varrho_2 - k_2 T_2^4 \\ 0 \\ k_4\varrho_4 - k_2 T_4^4 \\ 0 \\ 0 \\ 0 \end{pmatrix}, \; F(\rho) = \begin{pmatrix} \dot{Q} + k_3\varrho_1 \\ \dot{Q} + k_3\varrho_2 \\ \dot{Q} + k_5\varrho_1 + k_6 T_{\mathrm{E}}^4 \\ \dot{Q} + k_3\varrho_4 \\ \dot{Q} \\ \dot{Q} \\ 0 \end{pmatrix}, \tag{6c}$$

where $k_{01} = k_0 + k_1$, $k_1 = \varepsilon_{\mathrm{Al}}\,\sigma\,A_{\mathrm{F}}$, $k_2 = (\varepsilon_{\mathrm{sc}} - \varepsilon_{\mathrm{Al}})\,\sigma\,A_{\mathrm{F}}$, $k_3 = G_s\,a_{s,\mathrm{Al}}\,A_{\mathrm{F}}$, $k_4 = G_s\,(a_{s,\mathrm{sc}} - a_{s,\mathrm{Al}})\,A_{\mathrm{F}}$, $k_5 = p_{\mathrm{Af}}\,G_s\,a_{s,\mathrm{Al}}\,A_{\mathrm{F}}$, $k_6 = a_{\mathrm{IR,Al}}\,\sigma\,A_{\mathrm{F}}$ are auxiliary constants.

3. PID-based controller with heating power variations. As certain electronic and thermodynamic components of the CubeSat were generally designed for terrestrial applications, we require the spacecraft equipment to operate around room temperature. Furthermore, at room temperature, it is less expensive and much easier to conduct qualification and flight acceptance testing as well as equipment development [18]. Due to the varying mass, shape, and distribution of the payload, a spacecraft requires strong structural stability so a thermally-induced distortion has to be minimized or rigidly controlled. As a first step, a thermal mathematical model was built in [4] to analyse the thermal behaviour of the CubeSat system equipped with an additional propellant tank placed in the middle of the spacecraft. The possibility to regulate the fuel tank temperature to follow a prescribed constant temperature during the satellite orbital motion was examined in [5].

In a small satellite, the power of an active heater is often severely limited. Therefore, it is critical to determine precisely the minimum heating power required for a given control objective (even before the manufacturing of the spacecraft). In this section, we fix the solar panel coverage of the CubeSat to $\lambda = 0.3$, namely, 30% portion of the appropriate faces are covered by solar panels. Then, PID-based controllers are designed and simulated to find a minimum heating power required to lead and hold the tank temperature at $290K$. The leading concept in this study is the heat rate or flux $\dot{Q}_{\mathrm{c}}$, which is provided as thermal power by a heater (actuator) to the fuel tank. The heater attached to the fuel tank utilizes the control signal to produce the additional heat flux $\dot{Q}_{\mathrm{c}}$ along the shady part of the orbit.

To determine a feasible set of coefficients for the PID controller, we used Ziegler's and Nichols's rule. The obtained values for $K_P = 5$, $T_I = 1\mathrm{s}$, and $T_D = 1\mathrm{s}$ were used for all PID-based controller scheme. In order to find the minimum required heat flux Matlab/Simulink models have been implemented to simulate the CubeSat thermal dynamics controlled by PID-based controllers. During the analysis, two different PID strategies were considered. Firstly, the traditional PID control loop is applied with actuator saturation. Then, the control dynamics are supplemented by integral anti-windup feedback of the actuator's error. For both control schemes, the same conditions are considered to observe the fuel tank thermal responses among multiple heat fluxes values such as (1, 1.3, 1.5, and 2 W).

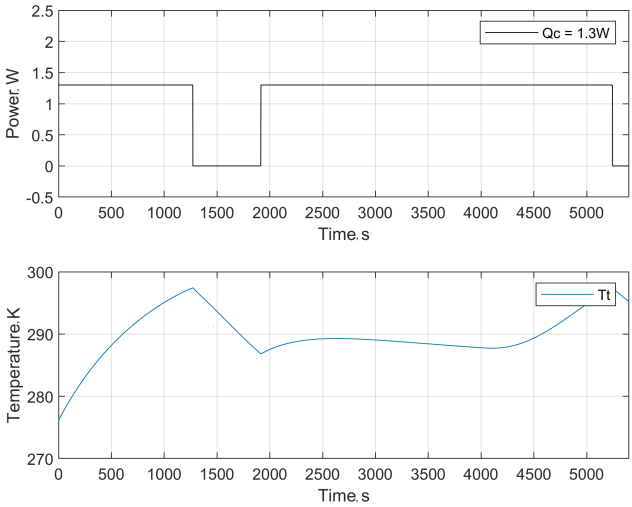

Fig. 2. Simulations for heat flux consumption limited at 1.3 W and the fuel tank thermal response via the PID controller within the limited heat flux

The simulation results corresponding to classical PID control with input saturation levels of $1.3W$ and $1.5W$ are shown in Figures 2 and 4, respectively, whereas, the results for anti-windup PID control are visible in Figures 3 and 5.

The simulation results show that the minimum heating power to achieve the prescribed control goals is about $1.5W$. Moreover, the results clearly show that the thermal response of the fuel tank, *corresponding to the anti-windup PID controller*, is more advantageous because of faster rising time and almost no overshoot.

4. Linearization-based control system. For the tank temperature control, a nonlinear control design technique is shown in this section using input/output feedback linearization as proposed in [6, 19, 20].

Hence, a feedback linearization law has been derived using the thermal mathematical model equations (1) considering the case of 70% aluminum and 30% solar cells ($\lambda = 0.3$) covering three faces of the satellite which are exposed to the sun throughout the circular satellite's orbit. It is important to limit the heat flux passed by the heater to the propellant tank at $1.5W$.

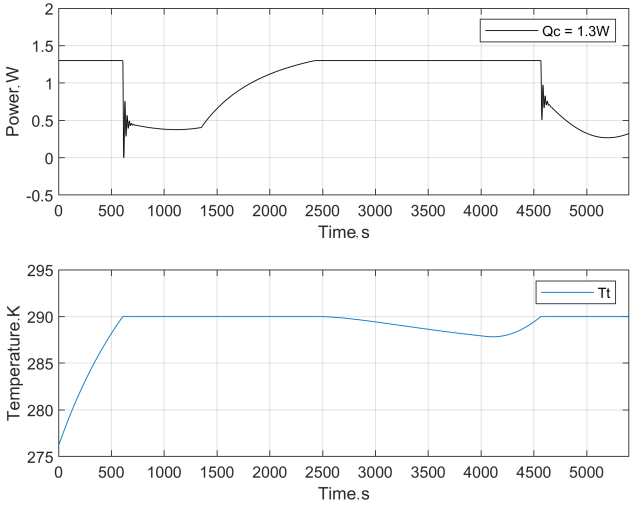

Fig. 3. Simulations for heat flux consumption limited at 1.3 W and the fuel tank thermal response via the Anti-windup PID controller within the limited heat flux

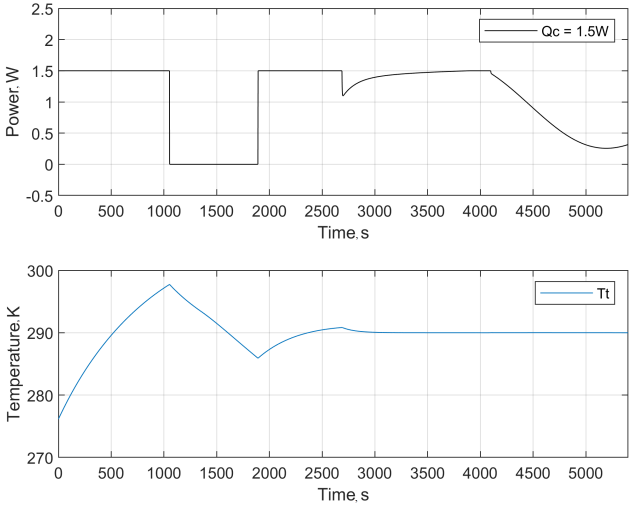

Fig. 4. Simulations for heat consumption limited at 1.5 W and the fuel tank thermal response via the PID controller within the limited heat flux

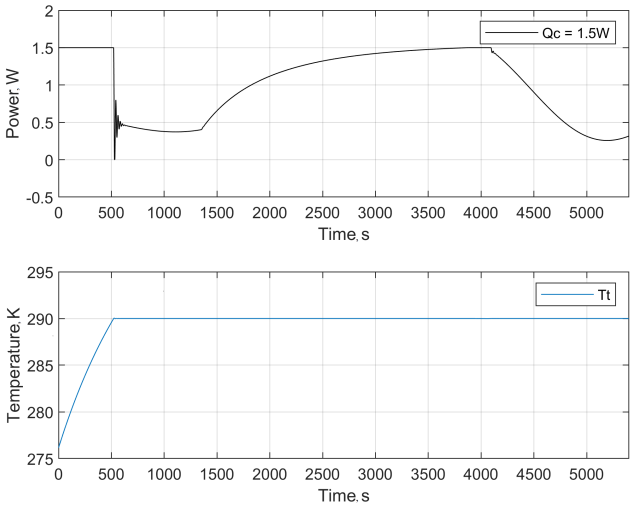

Fig. 5. Simulations for heat flux consumption limited at 1.5 W and the fuel tank thermal response via the Anti-windup PID controller within the limited heat flux

The dynamic equation of the tank's temperature is written as follows:

$$\dot{T}_{\mathrm{T}} = \frac{k_0}{k_{\mathrm{T}}}\left(\sum_{i=1}^{6} T_i^4 - 6T_{\mathrm{T}}^4\right) + \frac{1}{k_{\mathrm{T}}}u. \tag{7}$$

To perform a the feedback linearization, the following nonlinear input function is defined:

$$u = k_{\mathrm{T}}e_r - k_0\left(\sum_{i=1}^{6} T_i^4 - 6T_{\mathrm{T}}^4\right), \tag{8}$$

where $e_r = v_r - T_{\mathrm{T}}$ is the error signal, namely, the difference between T_{T} and the fuel tank reference temperature v_r. In this section, we considered $v_r = 290K$ in the simulations.

Observe that by substituting feedback (8) into (7) we obtain:

$$\dot{T}_{\mathrm{T}} = e_r. \tag{9}$$

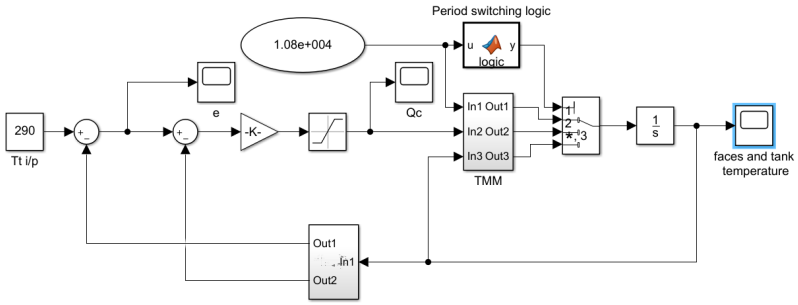

Fig. 6. Input/output linearization control framework in Matlab/Simulink

The Matlab/Simulink configuration presented in Figure 6 describes the fuel tank thermal control system via the input-output linearization structure. It is visible that the peak power delivered to the tank through the heater is 1.5 W, as presented in Figure 7 which satisfies the physical constraints see [4]. Figure 8 exposes the thermal behavior scheme of the propellant tank and the CubeSat surface.

5. Optimal parameter design using MPC. In this section, we present a simultaneous design for both a feasible control input signal ($\dot{Q}_{\mathrm{c}}$) and an optimal solar panel area (λA_{F}). To model and solve nonlinear MPC optimization problems we used MATLAB's Model Predictive Control Toolbox [27] (MPC-Toolbox), which is based on [16] and on the works (e.g., [32]) collected in [17].

5.1. Nonlinear MPC design. In this subsection, we present in brief the MPC optimization problem based on [32]. We consider a continuous-time nonlinear system

$$\dot{x}(t) = f(x(t), u(t), \rho(t)), \tag{10}$$

where x is the state vector, u is the input or the manipulated variable, and ρ is a known disturbance signal. We assume that the present and future values of ρ are both available.

Note that the MPC is a discrete-time controller, therefore, a sampled model of (10) is considered by the MPC-Toolbox [27, Pg. 10.4] by using the implicit trapezoidal method (i.e., the Tustin approximation) with a constant sampling period (h). Additionally, we consider a zero-order hold on the manipulated variable u (i.e., u is designed in the form of a staircase function). On the other hand, we assume that the known disturbance ρ is a piecewise

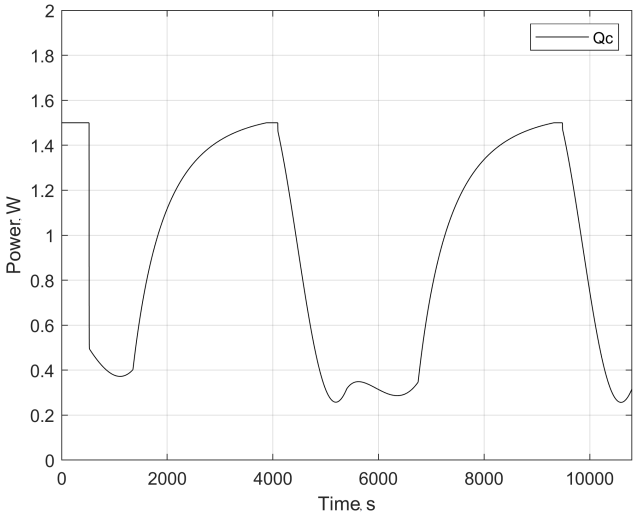

Fig. 7. The essential heat flux to regulate the fuel tank temperature via linearization-based controller

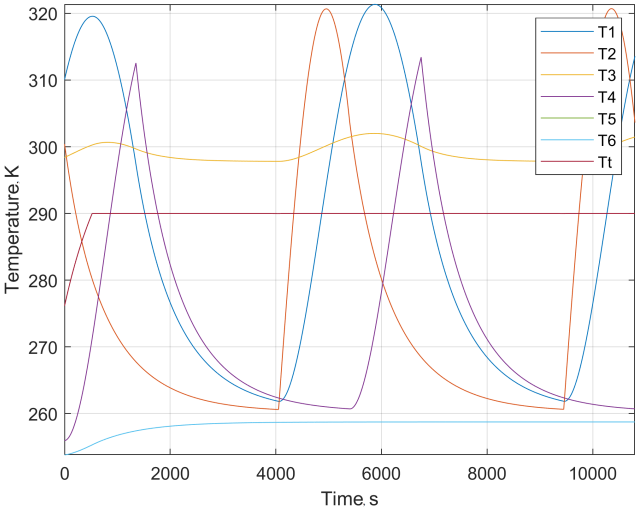

Fig. 8. CubeSat surface and its fuel tank thermal behaviors via linearization-based controller and heating power limited at 1.5 W

affine function, namely

$$\begin{aligned} &u(t) = u(t_k), \text{ for all } t \in [t_k, t_{k+1}), \text{ and} \\ &\rho(t) \approx \rho(t_k) + \frac{t - t_k}{h}(\rho(t_{k+1}) - \rho(t_k)), \text{ for all } t \in [t_k, t_{k+1}), \end{aligned} \tag{11}$$

where $t_k = k \cdot h$ for any integer number k. Then, the Tustin approximation of (10) simplifies to

$$\begin{aligned} x(t_{k+1}) \approx x(t_k) + \frac{h}{2}\Big(&f\big(x(t_k), u(t_k), \rho(t_k)\big) + \\ &+ f\big(x(t_{k+1}), u(t_k), \rho(t_{k+1})\big)\Big). \end{aligned} \tag{12}$$

Let $\hat{x}(t_{k+i}|t_k)$, $i = 1, \ldots, N$ denote the value of the state at time t_{k+i} *predicted* at the kth time step t_k using the discrete-time approximation (12) in the knowledge of $x(t_k)$, $\rho(t_k)$, $\ldots$, $\rho(t_{k+i})$ and for some input. Similarly, let $u(t_{k+i}|t_k)$, $i = 0, \ldots, N-1$ denote the value of the input at time t_{k+i} *computed* at the kth time step t_k. Integer number N constitutes the so-called *prediction horizon* of the MPC problem. Then, the MPC input design at time t_k can be formulated as follows.

Problem 1 (General MPC design). Consider a dynamical system (10).

Assume that the values of $x(t_k)$, $\rho(t_k)$, $\ldots$, $\rho(t_{k+N})$ are available at time t_k. Compute $\hat{x}(t_{k+i}|t_k)$, $i = 1, \ldots, N$ and $u(t_{k+i}|t_k)$, $i = 0, \ldots, N-1$, which minimize a cost function

$$J\big(\hat{x}(t_{k+1}|t_k), \ldots, \hat{x}(t_{k+N}|t_k), \hat{u}(t_k|t_k), \ldots, u(t_{k+N-1}|t_k)\big), \tag{13}$$

and satisfy the following equality constraints (prediction model):

$$\begin{cases} \hat{x}(t_{k+i+1}|t_k) = \hat{x}(t_{k+i}|t_k) + \\ \quad + \dfrac{h}{2}\Big(f\big(\hat{x}(t_{k+i}|t_k), u(t_{k+i}|t_k), \rho(t_{k+i})\big) + \\ \qquad + f\big(\hat{x}(t_{k+i+1}|t_k), u(t_{k+i}|t_k), \rho(t_{k+i+1})\big)\Big), \\ \hat{x}(t_k|t_k) = x(t_k). \end{cases} \tag{14}$$

We are allowed to enforce additional custom constraints on the designed input and the predicted state values, e.g., we can prescribe bounds for the state:

$$\underline{x} \leqslant x(t_{k+i}|t_k) \leqslant \overline{x} \text{ for all } i = 1, \ldots, N, \tag{15a}$$

or the rate of the input can also be bounded

$$\underline{\nu} \leqslant u(t_{k+i}|t_k) - u(t_{k+i-1}|t_k) \leqslant \overline{\nu} \text{ for all } i = 1, \ldots, N-1, \qquad (15b)$$

or, e.g., the input can be set constant on the prediction horizon ($u(t_{k+i}|t_k) = u(t_k|t_k)$ for all $i = 1, \ldots, N-1$). $\triangle$

Note that in Problem 1, both the predicted state $\hat{x}(t_{k+i}|t_k), i = 1, \ldots, N$ and the "planned" input $u(t_{k+i}|t_k)$, $i = 0, \ldots, N-1$ are considered as *free decision variables*, and they are meant to be found such that both the prediction model (14) and the prescribed control goals (e.g., (15)) are satisfied.

In a typical MPC design, a sequence of input values are computed *on-line* in each time-step t_k for a typically short prediction horizon (e.g., $N = 10$), and only the first computed input value $u(t_k|t_k)$ is applied to the system for all $t \in [t_k, t_{k+1})$. Then, a new computation is performed at t_{k+1} in the knowledge of the already measured new state value $x(t_{k+1})$, and again only $u(t_{k+1}|t_{k+1})$ is applied to the system on the next sampling interval $t \in [t_{k+1}, t_{k+2})$. Note that the on-line MPC design is applicable only if the processing time of the MPC optimization is less than the sampling period (h).

5.2. Optimal solar panel area computation. In this section, we propose an *off-line* MPC optimization to compute an optimal solar panel area. Differently from the on-line MPC, we compute a sequence of input values only at time step $k = 0$ and we consider a larger prediction horizon (e.g., $N = 40$, 60 or 100), which covers two consecutive orbital periods. Roughly speaking, after computing λ with an off-line MPC, we are ready to manufacture the satellite and control the temperatures by using, e.g., a PID controller or an on-line MPC. Note that our primary aim is to obtain an optimal/feasible λ, rather than to control the system, therefore, an on-line MPC design is not addressed for the thermal model of the CubeSat system.

Due to the fact that an optimal control sequence is computed only in t_0 ($k = 0$), the term "$|t_0$" is omitted from the arguments of $\hat{x}$ and u. The off-line MPC problem for the optimal λ computation is summarized as follows.
Problem 2 (Optimal λ computation). Consider a dynamical system (10), with

$$\begin{aligned} &x : [0, \infty) \to \mathbb{R}^7,\ x_j(t) = T_j(t), j = 1, \ldots, 6,\ x_7(t) = T_{\mathrm{T}}(t), \\ &u : [0, \infty) \to \mathbb{R}^2,\ u_1(t) = \dot{Q}_{\mathrm{c}}(t),\ u_2(t) = u_\lambda(t), \\ &\rho : [0, \infty) \to \mathbb{R}^3. \end{aligned} \qquad (16)$$

Assume that the values of $x(t_0), \rho(t_0), \ldots, \rho(t_N)$ are available at time $t_0 = 0$. Compute $\hat{x}(t_i)$, $i = 1, \ldots, N$ and $u(t_i)$, $i = 0, \ldots, N-1$, which

minimize the cost function

$$J\big(u(t_0)\big) = 1 - u_2(t_0), \tag{17}$$

satisfy the difference equation

$$\begin{cases} \hat{x}(t_{i+1}) = \hat{x}(t_i) + \dfrac{h}{2}\Big(f\big(\hat{x}(t_i), u(t_i), \rho(t_i)\big) + \\ \qquad\qquad + f\big(\hat{x}(t_{i+1}), u(t_i), \rho(t_{i+1})\big)\Big), \\ \hat{x}(t_0) = x(t_0), \end{cases} \tag{18}$$

and satisfy the following additional constraints

$$\begin{aligned} &1.\ \hat{x}_7(t_i) \in [\underline{T_{\mathrm{T}}}, \overline{T_{\mathrm{T}}}] \text{ for all } i = k_{(\mathrm{start})}, \ldots, N, \\ &2.\ \hat{x}_j(t_i) \leqslant \overline{T_{\mathrm{F}}} \text{ for all } j = 1, \ldots, 6 \text{ and all } i = 1, \ldots, N, \\ &3.\ u_1(t_i) \in [0, \overline{u}] \text{ for all } i = 1, \ldots, N-1, \\ &4.\ u_2(t_i) = u_2(t_0)\ (= \lambda) \text{ for all } i = 1, \ldots, N-1, \\ &5.\ u_2(t_0) \in [0, 1], \end{aligned} \tag{19}$$

where $\underline{T_{\mathrm{T}}}$, $\overline{T_{\mathrm{T}}}$, $\overline{T_{\mathrm{F}}}$, $\overline{u}$ and the integer number $k_{(\mathrm{start})}$ are constant scalar values given a priori. $\triangle$

Note that the quasi-LPV model formulation (5) of the thermal model does not fit into the model class (10) required by the MPC design, as the "input" λ appears on both sides of (5). Therefore, we consider the following relaxed quasi-LPV model:

$$\begin{aligned} \dot{x}(t) = I_k^{-1}(\lambda^*)\Big(&A(x(t))x(t) + Bu_1(t) + \\ &+ E(x(t), \rho(t))u_2(t) + F(\rho(t))\Big), \end{aligned} \tag{20}$$

where $u(t) = \begin{pmatrix} \dot{Q}_{\mathrm{c}}(t) \\ \lambda \end{pmatrix}$ and the parameter λ^* is assumed to be known before the optimization. Note that dynamics (20) are equivalent to (5) if and only if $\lambda^* = \lambda$.

To find an optimal value for λ, we iteratively approximate $\lambda^* \approx \lambda$ as follows. Consider an initial value $\lambda^*_{(0)}$ for λ^*. In the κth iteration, we perform the MPC optimization described in Problem 2 for $\lambda^* = \lambda^*_{(\kappa)}$. If the resulting optimal value for $\lambda = u_\lambda(t_0)$ is not "close enough" to $\lambda^*_{(\kappa)}$ (e.g., $|\lambda - \lambda^*_{(\kappa)}| > \varepsilon_\lambda$), we perform again the optimization with $\lambda^*_{(\kappa+1)} = \lambda$.

5.3. Numerical simulations and results. The computations presented in this section were processed on a laptop with Intel Core i7-4710MQ CPU at 2.50 GHz and 16 GB of RAM.

During the analysis, we considered six different case studies with different sampling rates (h), and control objectives ($\underline{T_{\mathrm{T}}}$, $\overline{T_{\mathrm{T}}}$, $\overline{u}$, $k_{(\mathrm{start})}$), but with a common value for $\overline{T_{\mathrm{F}}} = 370\mathrm{K}$, and $\lambda^*_{(0)} = 0.5$ with $\varepsilon_\lambda = 0.0005$. In each case study, the MPC design is performed over two orbital periods with sampling rate $h = \frac{2P}{N}$. As presented in Section 5.1, the input is searched in the form of a staircase function during the optimization, whereas, the external known disturbance function is assumed to be a piecewise linear function in time. After the optimization, the thermal model (5) of the CubeSat system is simulated with the computed control input sequence $u_1(t_i)$, $i = 0, \ldots, N-1$ and the optimal λ with the assumption that the input is *piecewise linear* between the computed discrete values $u(t_i)$, namely:

$$\begin{aligned} \bar{u}_1(t) = u_1(t_i) + \frac{t - t_i}{h}(u_1(t_{i+1}) - u_1(t_i)), \\ \text{for all } t \in [t_i, t_{i+1}), \\ i = 0, \ldots, N-1. \end{aligned} \tag{21a}$$

Differently from the MPC optimization, the simulation is performed on four consecutive orbital periods. Therefore, the control input sequence for the second orbital period computed through the MPC optimization is periodically extended in the simulation for the next two consecutive orbital periods, namely:

$$\bar{u}_1(t) = \bar{u}_1\big(t - (\ell - 1)P\big), \text{ for all } t \in [\ell P, (\ell + 1)P),\ \ell = 2, 3. \tag{21b}$$

Let $\bar{x}(t_i)$ denote the simulated state at time t_i of the state-space model (5) driven by the computed input signal $\bar{u}(t)$ in (21). In order to quantify the prediction error of the MPC design with respect to the simulated time evaluation of the tank temperature, we compute the following two error quantities:

$$\begin{aligned} \text{MSE}: \ & \tfrac{1}{N}\textstyle\sum_{i=1}^{N}(\hat{x}_7(t_i) - \bar{x}_7(t_i))^2, \\ \text{abs. err.}: \ & \max_{i=1,\ldots,N} |\hat{x}_7(t_i) - \bar{x}_7(t_i)|. \end{aligned} \tag{22}$$

The abbreviation MSE designates the mean squared error between the predicted and simulated values of the tank temperature in the discrete time points t_i, $i = 1, \ldots, N$. Whereas, the absolute error (abs. err.) is the maximal absolute value of the difference between predicted and simulated value of the tank temperature in the discrete time points over the prediction horizon.

The MPC optimization results for the six different case studies are presented in details in Figures 9-14, respectively. Each of Figures 9-14 comprises six subplots (A)-(F), which illustrate the following results: subplot (A) presents the optimal staircase control input sequence $u_1(t_i) = \dot{Q}_{\mathrm{c}}(t_i)$, $i = 0, \ldots, N-1$, computed through the MPC optimization; subplot (B) shows the predicted values of the tank temperature at $t_0, \ldots, t_N$ (blue dotted line), and the interval constraint on $T_{\mathrm{T}}(t_i) \in [\underline{T_{\mathrm{T}}}, \overline{T_{\mathrm{T}}}]$ for all $i = k_{(\mathrm{start})}, \ldots, N$ (red region); subplot (C) illustrates the predicted values $T_j(t_i)$ of the surface temperatures at $t_0, \ldots, t_N$, and $j = 1, \ldots, 6$; subplot (D) illustrates the interpolated piecewise affine input function (21) considered in the simulations; in Subplot (E), the simulated time evaluation of the tank temperature is compared against the predicted time series of the tank temperature through the mean squared and absolute prediction errors (22); subplot (F) illustrates the simulated time evaluation of the surface temperatures.

The presented data in subplot (A)-(C) are computed through the MPC optimization, and they span two orbital periods. The data in (D)-(F) present the simulation results of the thermal model (5) driven by the input (21). In order to promote the readability of this section, Figures 9-14 are tabulated to the end of this paper. The precise calculation results and source code are available on-line [33].

In Figure 9, we present the first case study. We designed an optimal value for the solar panel area and a controller sequence to keep the tank temperature around 290 K. If we allow higher fluctuation $T_{\mathrm{T}}(t_i) \in [287, 293]$ K, $i = 3, \ldots, N$, ($N = 40$, $h = 270$s), but require a low power control signal ($\overline{u} = 1.2$ W), we obtain $\lambda \simeq 0.51$. In the second case study (Figure 10), we restricted the tank temperature to a tighter interval $T_{\mathrm{T}}(t_i) \in [289, 291]$ K. The optimization points out that the solar panel ratio should be decreased to $\lambda = 0.4481$, at the same time, the applicable heating power limit should be increased to $\overline{u} = 1.4$ W (Figure 10). It is worth remarking that the control objectives are more conservative in this case compared to the first case study. Therefore, we considered a shorter sampling period $h = 180$s ($N = 60$). Observing the results of the first two control design setups, we can conclude that the smaller temperature fluctuation can be achieved, if the solar panel area is small enough, and the actuator has a higher power limit to be able to provide the necessary heat flux during the shady parts of the orbit.

In the next two cases, our major objective is to analyse the precision and complexity of the proposed optimization method for two different sampling periods. In these computations, the baseline tank temperature was raised to 300 K, and we allowed ± 3 K fluctuation (namely, $\underline{T_{\mathrm{T}}} = 297$ K, and $\overline{T_{\mathrm{T}}} = 303$ K). First, we considered a longer sampling period $h = 270$s ($N = 40$),

secondly, we used a shorter one $h = 108$s ($N = 100$). In both cases, one feasible power bound for the heater was $\overline{u} = 1.75\,\mathrm{W}$. As Figures 11 and 12 illustrate, a shorter sampling period may result in a more precise prediction model (18). Obviously, the undershoot and overshoot from the allowed (red) region is lower if a shorter sampling period is selected. Unfortunately, the computational complexity of the optimization increases combinatorially as we consider a longer prediction horizon (i.e., a larger $N = \frac{2P}{h}$).

From the authors experience, the bound conditions for the surface temperatures ($\hat{x}_j(t_i) \leqslant 370\,\mathrm{K}$ for all $i = 1, \ldots, N$, and all $j = 1, 6$) are trivially satisfied in the previous four cases (Figures 9-12). Therefore, this constraint is removed from the optimization to reduce its computational complexity.

Another pair of interesting experiments are illustrated in Figure 13 and 14. Let us relax the upper bound for the CubeSat's surface and tank temperature $\overline{T_{\mathrm{F}}} = \overline{T_{\mathrm{T}}} = \infty$. (In the numerical computations we consider finite but "large enough" value for $\overline{T_{\mathrm{T}}} = 330\,\mathrm{K}$.) Using MPC, we can find the lowest feasible upper bound $\overline{u}$ for the input power, such that the heater can maintain the tank's temperature above $\underline{T_{\mathrm{T}}}$. The optimization was performed in two different cases for $\underline{T_{\mathrm{T}}} = 290\,\mathrm{K}$ and $\underline{T_{\mathrm{T}}} = 297\,\mathrm{K}$. Through the optimization, we concluded that the CubeSat's appropriate faces should be completely covered by solar cells ($\lambda = 1$), and the minimum required upper bound for the thermal flux should be $\overline{u} = 1.069$ and $\overline{u} = 1.545$, respectively. However, we have seen in the previous syntheses that in the real-word scenario, $\lambda = 1$ is not a feasible value for the solar panel coverage. In this case, the parts of the satellite will be overheated, and we are not able to give a control input sequence that keeps the faces and the tank temperature below the prescribed values, i.e., the optimization is infeasible with the criteria $\hat{x}_j(t_i) \leqslant 370\,\mathrm{K}$ for all $i = 1, \ldots, N$, and all $j = 1, 6$.

Although the on-line MPC design is planned as a future work, we remark that the dynamics of the CubeSat's thermal system are relatively slow, therefore, the processing time of the "off-line" MPC can be easily kept much below the sampling period. From the second case study (Figure 10, we have found that for a relatively large prediction horizon ($N = 60$) the optimization can still be executed (comfortably) within a single sampling period.

6. Conclusion. In this paper, control approaches were presented for the thermal system of an orbiting CubeSat. During its orbital motion, the satellite flies along the sunny and shady sides of the Earth. Therefore, periodic fluctuation can be observed in the thermal dynamics of the different components of the CubeSat. To maintain the tank temperature within an admissible range, a passive control approach was presented in [4] by manipulating the surface

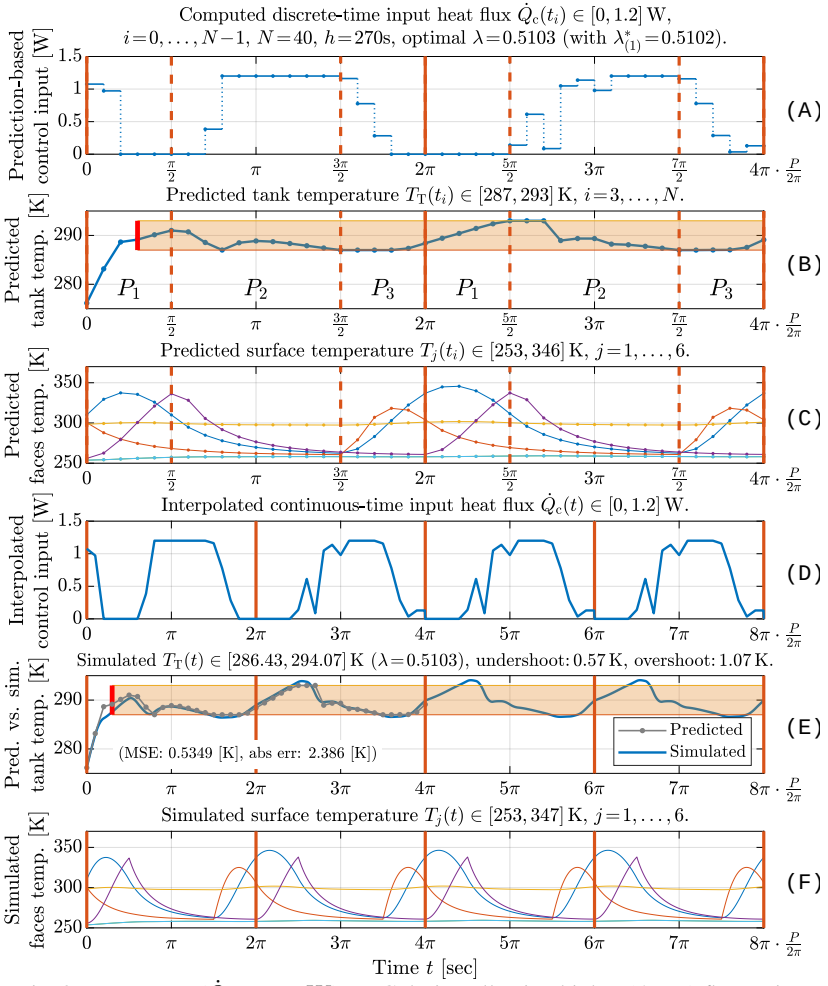

Fig. 9. Low power ($\dot{Q}_c \leqslant 1.2\ W$) MPC design allowing higher (± 3 K) fluctuation around $T_T = 290$ K with $h = 270$s, $N = 40$. The final value of λ^* was obtained through two iterations: $\lambda^*_{(0)} = 0.5$, $\lambda^*_{(1)} = 0.5102$. The processing time of the MPC optimization was less than 15 seconds. The constraints (18) and (19) were tested less than 500 times during the optimization

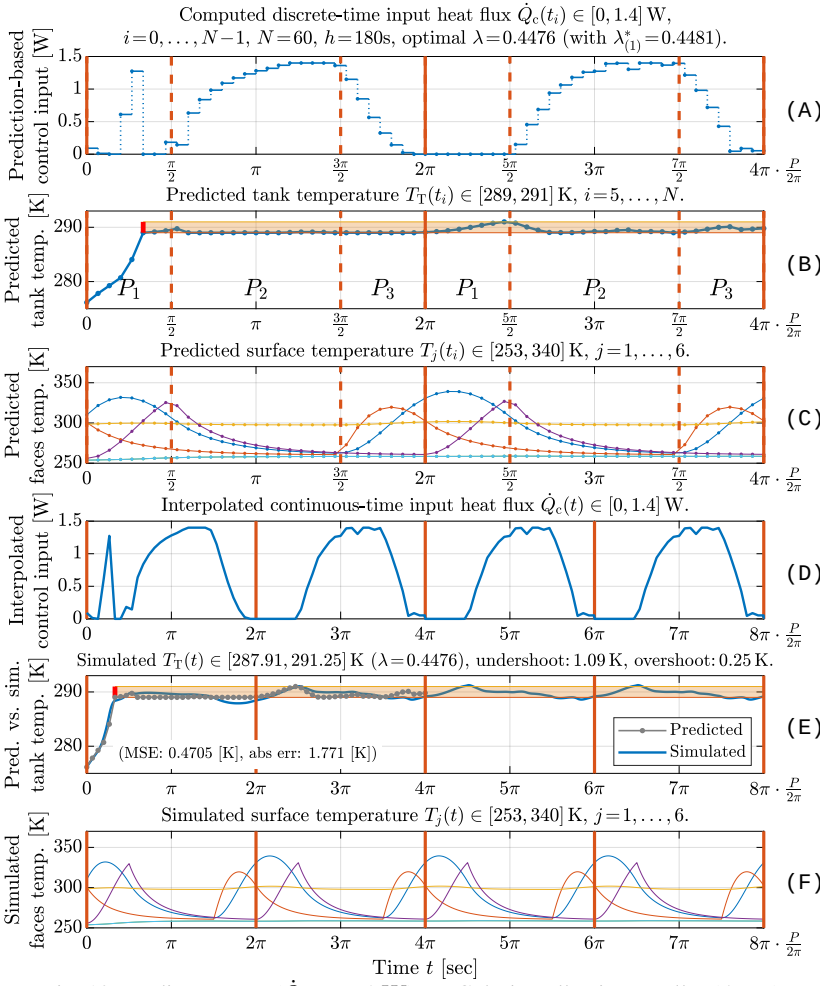

Fig. 10. Medium power ($\dot{Q}_c \leqslant 1.4\ W$) MPC design allowing smaller (± 1 K) fluctuation around $T_T = 290$ K with $h = 180$s, $N = 60$. The final value of λ^* was obtained through two iterations: $\lambda^*_{(0)} = 0.5$, $\lambda^*_{(1)} = 0.4481$. The processing time of the MPC optimization was less than 40 seconds. The constraints (18) and (19) were tested less than 750 times during the optimization

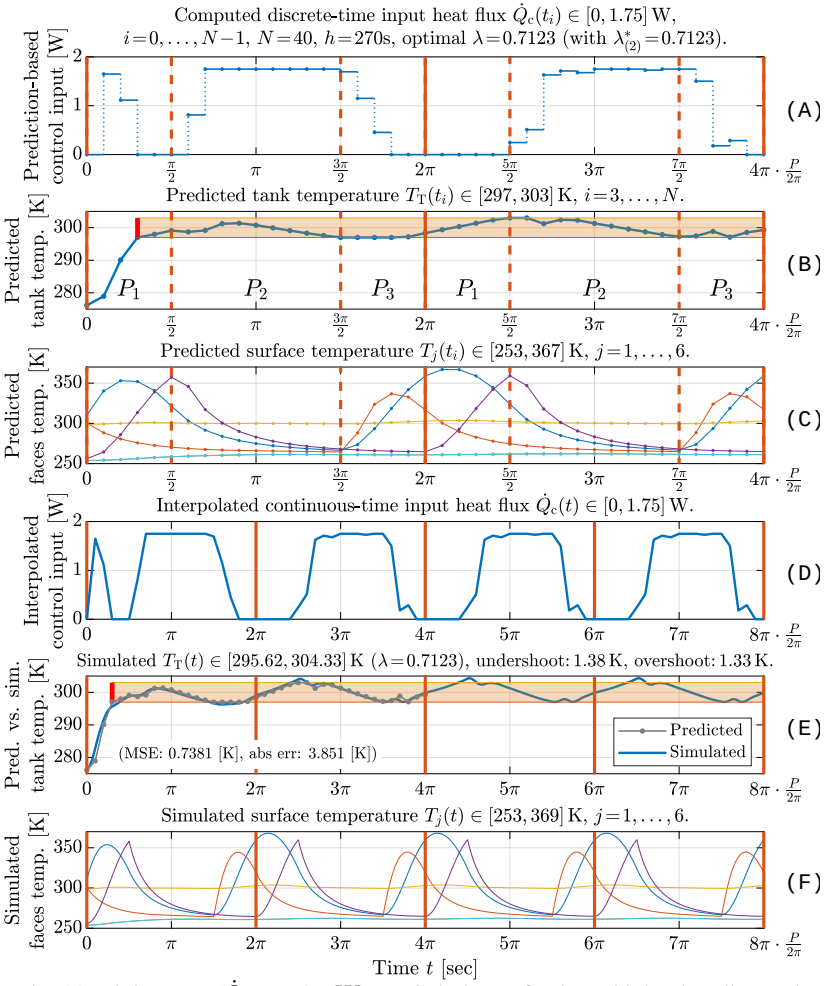

Fig. 11. High power ($\dot{Q}_c \leqslant 1.75\ W$) MPC design enforcing a higher baseline tank temperature ($T_T = 300$ K) but allowing higher (± 3 K) fluctuation ($h = 270$s, $N = 40$). The final value of λ^* was obtained through three iterations: $\lambda^*_{(0)} = 0.5$, $\lambda^*_{(1)} = 0.7095$, $\lambda^*_{(2)} = 0.7123$. The processing time of the MPC optimization was less then 15 seconds. The constraints (18) and (19) were tested less than 550 times during the optimization

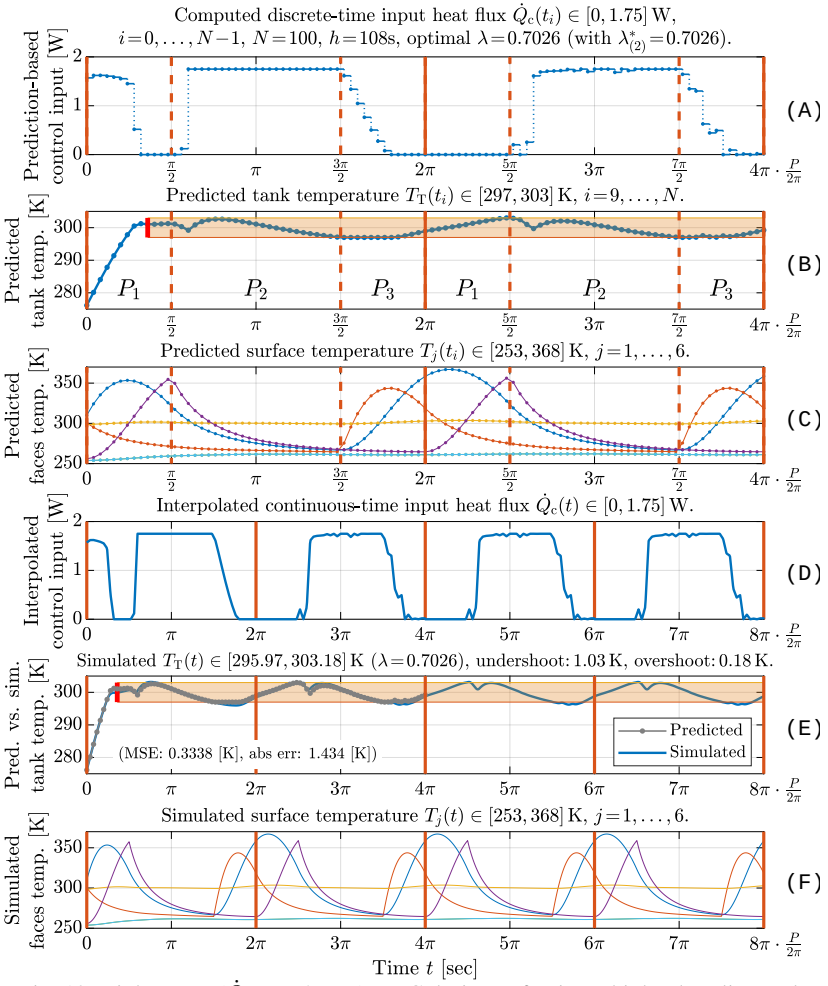

Fig. 12. High power ($\dot{Q}_c \leqslant 1.75$ W) MPC design enforcing a higher baseline tank temperature ($T_T = 300$ K) but allowing higher (± 3 K) fluctuation ($h = 108$s, $N = 100$). The final value of λ^* was obtained through three iterations: $\lambda^*_{(0)} = 0.5$, $\lambda^*_{(1)} = 0.7$, $\lambda^*_{(2)} = 0.7026$. The processing time of the MPC optimization was less than 200 seconds. The constraints (18) and (19) were tested less than 650 times during the optimization

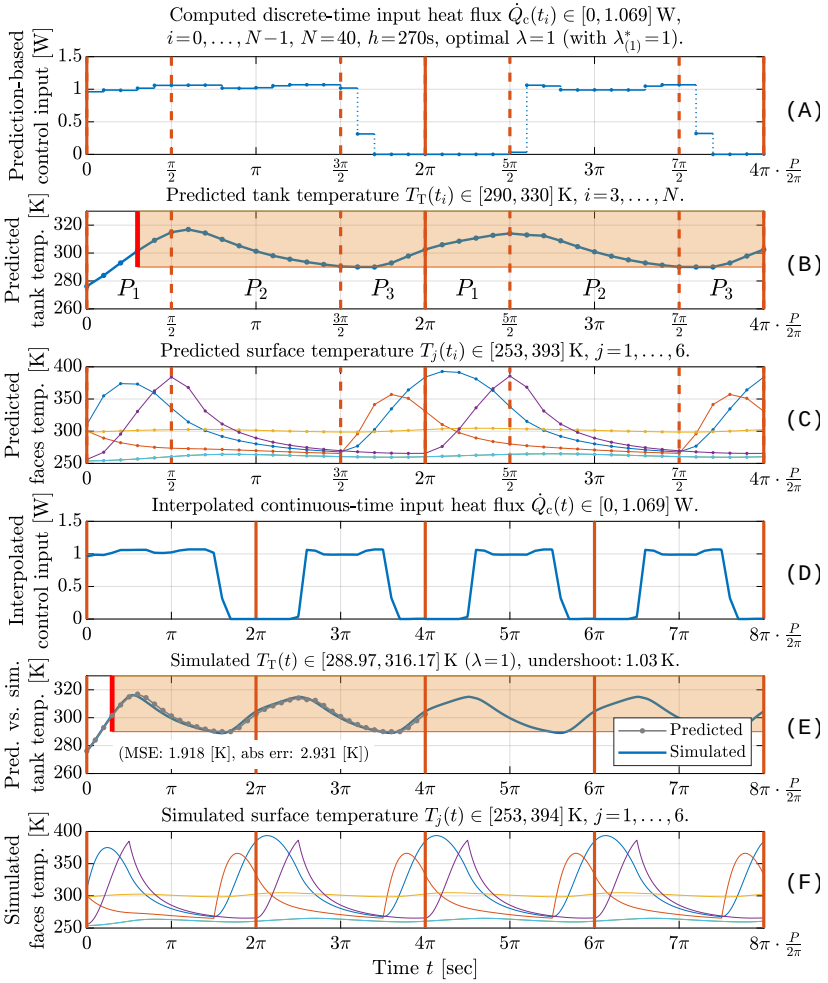

Fig. 13. Minimum thermal flux required to keep the tank's temperature above 290 K if $\lambda = 1$ (i.e., the appropriate faces of the CubeSat are fully covered by the solar panel). The sampling period is $h = 270$s, the prediction horizon is $N = 40$. The final value of λ^* was obtained through two iterations: $\lambda^*_{(0)} = 0.5$, $\lambda^*_{(1)} = 1$. The processing time of the MPC optimization was less than 1 second. The constraints (18) and (19) were tested 30 times during the optimization

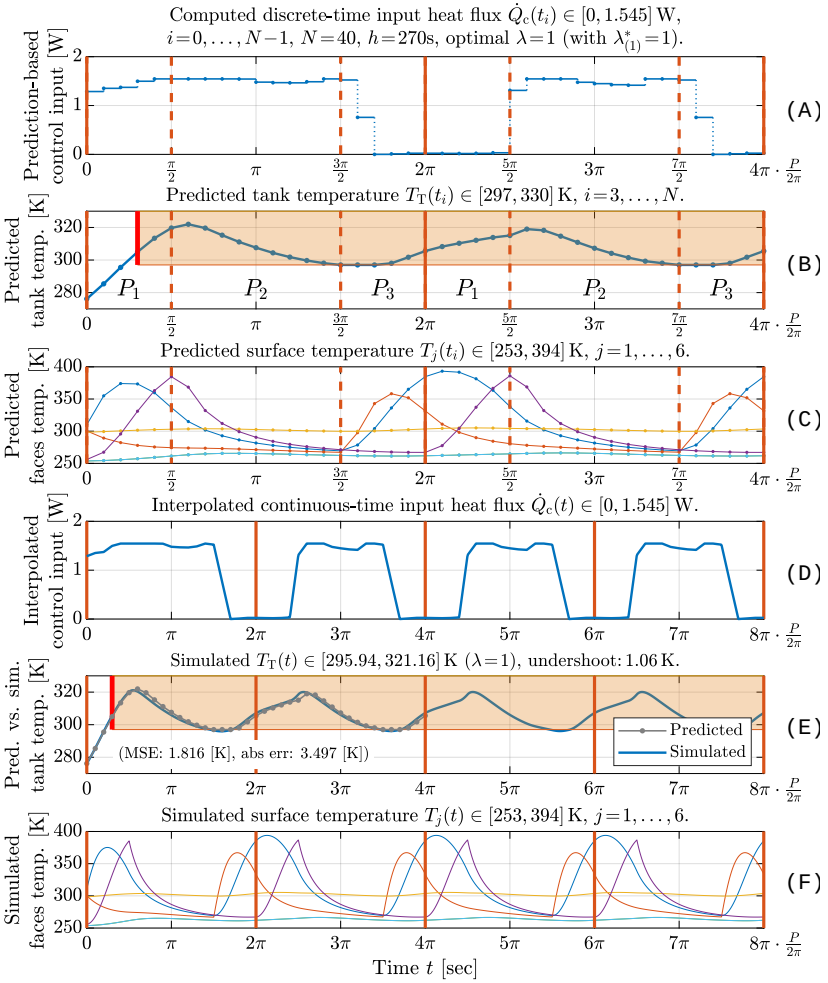

Fig. 14. Minimum thermal flux required to keep the tank's temperature above 297 K if $\lambda = 1$ (i.e., the appropriate faces of the CubeSat are fully covered by the solar panel). The sampling period is $h = 270$s, the prediction horizon is $N = 40$. The final value of λ^* was obtained through two iterations: $\lambda^*_{(0)} = 0.5$, $\lambda^*_{(1)} = 1$. The processing time of the MPC optimization was less than 1 second. The constraints (18) and (19) were tested 12 times during the optimization

coating of the CubeSat and the power dissipated heat flux of the on-board electrical devices. Differently from [4], here we proposed a simultaneous design for both passive and active control by selecting an optimal area for the solar panels (passive control) and computing a feasible heat flux signal (active control). Throughout the paper, we tested three different control design techniques to track a given reference tank temperature by considering multiple input saturation levels and solar panel coverage. First, we have fixed the area of the solar panels, and tested different heater power saturation levels in the classical PID controller scheme with an anti-windup compensation. Then, a feedback linearization technique has been applied to achieve reference tracking. In both control schemes, the simulations showed a time response which is technologically acceptable for the CubeSat's thermal system. The main contribution of the paper constitutes an optimization-based model-predictive approach for the simultaneous design of an optimal solar panel ratio and a feasible control input sequence. Through multiple MPC design scenarios, we demonstrated that an off-line model-predictive analysis is particularly useful for assessing the physical limits of the control. This is especially true for nonlinear models, where the set of available analysis and control design techniques is more limited compared to the results for linear time-invariant systems.

References

1. Mehrparvar A. et al. CubeSat design specification(CDS) REV 13. The CubeSat Project, San Luis Obispo, CA. 2014. pp. 1–42.
2. Cheney L.J. Development of safety standards for CubeSat propulsion systems. Faculty of California Polytechnic State University. 2014. 215 p.
3. Lemmer K. Propulsion for CubeSats. *Acta Astronautica*. 2017. vol. 134. pp 231–243.
4. Al-hemeary N., Jaworski M., Kindracki J., Szederkényi G. Thermal model development for a CubeSat. *Hungarian Journal of Industry and Chemistry*. 2019. pp. 25–32.
5. Al-hemeary N., Szederkényi G. Fuel tank temperature control of a time-varying CubeSat model. IEEE 17th World Symposium on Applied Machine Intelligence and Informatics. 2019. pp. 339–344.
6. Isidori A. Nonlinear control systems. Springer-Verla. 1995. 549 p.
7. Cox P.B. Towards efficient identification of linear parameter-varying state-space models. PhD dissertation, Eindhoven University of Technology. 2018. 354 p.
8. Mohammadpour J., Scherer C.W. Control of linear parameter varying systems with applications. Springer Science & Business Media. 2012. 550 p.
9. Rotondo D., Nejjari F., Puig V. Quasi-LPV modeling, identification and control of a twin rotor MIMO system. *Control Engineering Practice*. 2013. vol. 21. no. 6. pp. 829–846.
10. Atam E., Mathelin L., Cordier L. A hybrid approach for control of a class of input-affine nonlinear systems. *Int. J. Innov. Comput., Inf. Control*. 2014. vol. 10. no. 3. pp. 1207–1228.
11. Tu K.H., Shamma J.S. Nonlinear gain-scheduled control design using set-valued methods. Proceedings of the 1998 American Control Conference. ACC (IEEE Cat. No. 98CH36207). 1998. vol. 2. pp. 1195–1199.
12. Hoffmann C. Linear parameter-varying control of systems of high complexity. Technische Universität Hamburg-Harburg. 2016. 402 p.

13. Shin J.Y. Quasi-linear parameter varying representation of general aircraft dynamics over non-trim region. National Institute of Aerospace. 2007. 32 p.
14. Cisneros P.S.G., Voss S., Werner H. Efficient nonlinear model predictive control via quasi-LPV representation. 2016 IEEE 55th Conference on Decision and Control (CDC). 2016. pp. 3216–3221.
15. Marcos A., Balas G.J. Development of linear-parameter-varying models for aircraft. *Journal of Guidance, Control, and Dynamics*. 2004. vol. 27. no. 2. pp. 218–228.
16. Kouvaritakis B., Cannon M. Nonlinear predictive control: theory and practice. 2001.
17. Allgöwer F., Zheng A. Nonlinear Model Predictive Control. Birkhäuser. 2000. 472 p.
18. Cisneros P.S.G., Werner H. Stabilizing model predictive control for nonlinear systems in input-output quasi-LPV form. 2019 American Control Conference (ACC). 2019. pp. 1002–1007.
19. Abbas H.S., Hanema J., Tóth R., Mohammadpour J., Meskin N. An improved robust model predictive control for linear parameter-varying input-output models. *International Journal of Robust and Nonlinear Control*. 2018. vol. 28. no. 3. pp. 859–880.
20. Cisneros P.S.G., Voss S., Werner H. Efficient nonlinear model predictive control via quasi-LPV representation. 2016 IEEE 55th Conference on Decision and Control (CDC). 2016. pp. 3216–3221.
21. Abbas H.S. et al. A robust MPC for input-output LPV models. *IEEE Transactions on Automatic Control*. 2016. vol. 61. no. 12. pp. 4183–4188.
22. Hanema J., Tóth R., Lazar M. Stabilizing non-linear MPC using linear parameter-varying representations. 2017 IEEE 56th Annual Conference on Decision and Control (CDC). 2017. pp. 3582–3587.
23. Camacho E.F and Alba C.B. Model predictive control. Springer Science & Business Media. 2013. 405 p.
24. Maciejowski J.M. Predictive control: with constraints. Pearson education. 2002. 353 p.
25. Rossiter J.A. Model-based predictive control: a practical approach. CRC press. 2017. 344 p.
26. Rawlings J.B., Mayne D.Q. Model Predictive Control: Theory and Design. Nob Hill Publishing. 2010. 544 p.
27. Bemporad A., Ricker N.L., Morari M. Model Predictive Control Toolbox User's Guide. The MathWorks, 2019. 37 p.
28. Al-hemeary N., Szederkényi G. Power regulation and linearization-based control design of a small satellite. 2019 12th International Conference on Developments in eSystems Engineering 2019. pp. 646–650.
29. Fortescue P., Swinerd G., Stark J. Spacecraft systems engineering. John Wiley & Sons. 2011. 724 p.
30. Różowicz S., Zawadzki A. Input-output transformation using the feedback of nonlinear electrical circuits: Algorithms and linearization examples. *Mathematical Problems in Engineering*. 2018. vol. 2018. 13 p.
31. Cheng D., Isidori A., Respondek W., Tarn T.J. Exact linearization of nonlinear systems with outputs. *Mathematical systems theory*. 1988. vol. 21. no. 1. pp. 63–83.
32. Zheng A. Some practical issues and possible solutions for nonlinear model predictive control. Nonlinear Model Predictive Control. 2000. pp. 129–143.
33. Polcz P. Optimal solar panel area computation for a CubeSat system using an offline MPC design. GitHub repository. 2020 Available at: https://github.com/ppolcz/CubeSat_optimal_sparea (accessed: 02.03.2020)

Al-Hemeary Nawar — Ph.D student, Faculty of Information Technology and Bionics, Pázmany Péter Catholic University; Lecturer, Faculty of Electromechanical Engineering, University of technology, Iraq. Research interests: aerospace systems, CubeSat, nonlinear MPC. The number of publications – 3. al.hemeary@itk.ppke.hu; 50/A, Práter str., 1083, Budapest, Hungary; office phone: 003618864700/760.

Polcz Péter — Ph.D. candidate, Faculty of Information Technology and Bionics, Pázmany Péter Catholic University. Research interests: analysis and control of nonlinear systems, nonlinear MPC. The number of publications – 9. polcz.peter@itk.ppke.hu; 50/A, Práter str., 1083, Budapest, Hungary; office phone: 003618864700/759.

Szederkényi Gábor — Ph.D., Dr.Sci., Professor, Doctor of the Hungarian Academy of Sciences, Full professor, Faculty of Information Technology and Bionics, Pázmany Péter Catholic University. Research interests: nonnegative and kinetic systems, analysis and control of nonlinear systems, system identification, nonlinear MPC. The number of publications – 131. szederkenyi.gabor@itk.ppke.hu; 50/A, Práter str., 1083, Budapest, Hungary; office phone: 003618864751.

Acknowledgements. This work has been partially supported by the European Union, co-financed by the European Social Fund through the grant EFOP-3.6.3-VEKOP-16-2017-00002. The support of the University of Technology-Baghdad is also acknowledged. Szederkényi G. acknowledges the support of the project NKFIH 131545.

УДК 006.72 **DOI** 10.15622/sp.2020.19.3.4

Н. Аль -Хемеари, П. Полц, Г. Седеркеньи

ОПТИМАЛЬНЫЙ РАСЧЕТ ПЛОЩАДИ СОЛНЕЧНОЙ ПАНЕЛИ И ОТСЛЕЖИВАНИЕ ТЕМПЕРАТУРЫ ДЛЯ СИСТЕМЫ CUBESAT С ИСПОЛЬЗОВАНИЕМ УПРАВЛЕНИЯ ПРОГНОЗИРУЮЩИМИ МОДЕЛЯМИ

Аль-Хемеари Н., Полц П., Седеркеньи Г. **Оптимальный расчет площади солнечной панели и отслеживание температуры для системы CubeSat с использованием управления прогнозирующими моделями.**

Аннотация. В последнее время в аэрокосмическом сообществе, включая космические агентства, предприятия и научные центры, резко возрос интерес к небольшим спутникам, таким как CubeSats, из-за их экономичной работы. Также наблюдается проблема обеспечения точности работы спутников с минимальными затратами и энергопотреблением. Для маневренности CubeSat оснащен топливным баком, в котором топливо должно поддерживаться в соответствующем температурном режиме. Одновременно должно быть максимально увеличено производство энергии, чтобы другие компоненты спутника не перегревались. В целях удовлетворения технологическим требованиям предлагается многокритериальная схема оптимального управления с использованием нелинейной динамической тепловой модели системы CubeSat. Схема управления ПИД-регулятора с компенсацией интегрального насыщения используется для оценки минимального теплового потока, необходимого для поддержания заданной эталонной температуры топливного бака, а контроллер на основе линеаризации предназначен для контроля температурного режима. Оптимизация площади солнечного элемента и управления ограничением температуры представляется как проблема управления с прогнозирующими интегрированными нелинейными моделями с использованием формы квазилинейного регулирования параметров уравнений состояния. Для оценки положительных и отрицательных сторон конструкции управления и применимости подхода приведены несколько сценариев моделирования для разных пределов мощности и случаев покрытия солнечных элементов.

Ключевые слова: аэрокосмические системы, CubeSat, нелинейный УПМ, мощность привода, нелинейная динамическая модель, линеаризация обратной связи.

Аль-Хемеари Навар — аспирант, факультет информационных технологий и бионики, Католический университет Петера Пазманя; преподаватель, факультет электромеханического проектирования, Технологический университет, Ирак. Область научных интересов: аэрокосмическая система, кубсат, нелинейное управление по модели предсказания, мощность привода, нелинейная динамическая модель, линеаризация обратной связи. Число научных публикаций — 3. al.hemeary@itk.ppke.hu; ул. Пратер, 50/A, 1083, Будапешт, Венгрия; р.т.:. 0036205293922.

Полц Петер — аспирант, факультет информационных технологий и бионики, Католический университет Петера Пазманя. Область научных интересов: аэрокосмическая система, кубсат, нелинейное управление по модели предсказания, мощность привода, нелинейная динамическая модель, линеаризация обратной связи. Число научных публикаций — 9. polcz.peter@itk.ppke.hu; ул. Пратер, 50/A, 1083, Будапешт, Венгрия; р.т. :. 0036308285485.

Седеркеньи Габор — д-р техн. наук, профессор, доктор Венгерской академии наук, профессор, факультет информационных технологий и бионики, Католический университет Петера

Пазманя. Область научных интересов: аэрокосмическая система, кубсат, нелинейное управление по модели предсказания, мощность привода, нелинейная динамическая модель, линеаризация обратной связи. Число научных публикаций — 131. szederkenyi.gabor@itk.ppke.hu; ул. Пратер, 50/A, 1083, Будапешт, Венгрия; р.т.: + 36-1-886-4751.

Поддержка иследований. Работа выполнена при частичной финансовой поддержке Европейского Союза и Европейского социального фонда (грант EFOP-3.6.3-VEKOP-16-2017-00002). Также при поддержке Технологического университета Багдада и гранта NKFIH 131545 (руководитель гранта – Г. Седеркеньи).

Литература

1. Mehrparvar A. et al. CubeSat design specification (CDS) REV 13 // The CubeSat Project, San Luis Obispo, CA. 2014. pp. 1–42.
2. Cheney L.J. Development of safety standards for CubeSat propulsion systems // Faculty of California Polytechnic State University. 2014. 215 p.
3. Lemmer K. Propulsion for CubeSats // Acta Astronautica. 2017. vol. 134. pp. 231–243.
4. Al-Hemeary N., Jaworski M., Kindracki J., Szederkényi G. Thermal model de-velopment for a CubeSat // Hungarian Journal of Industry and Chemistry. 2019. pp. 25–32.
5. Al-Hemeary N., Szederkényi G. Fuel tank temperature control of a time-varying CubeSat model // IEEE 17th World Symposium on Applied Machine Intelli-gence and Informatics. 2019. pp. 339–344.
6. Isidori A. Nonlinear control systems // Springer-Verla. 1995. 549 p.
7. Cox P.B. Towards efficient identification of linear parameter-varying state-space models // PhD dissertation, Eindhoven University of Technology. 2018. 354 p.
8. Mohammadpour J., Scherer C.W. Control of linear parameter varying systems with applications // Springer Science & Business Media. 2012. 550 p.
9. Rotondo D., Nejjari F., Puig V. Quasi-LPV modeling, identification and control of a twin rotor mimo system // Control Engineering Practice. 2013. vol. 21. no. 6. pp. 829–846.
10. Atam E., Mathelin L., Cordier L. A hybrid approach for control of a class of input-affine nonlinear systems // Int. J. Innov. Comput., Inf. Control. 2014. vol. 10. no. 3. pp. 1207–1228.
11. Tu K.H., Shamma J.S. Nonlinear gain-scheduled control design using set-valued methods // Proceedings of the 1998 American Control Conference. ACC (IEEE Cat. No. 98CH36207). 1998. vol. 2. pp. 1195–1199.
12. Hoffmann C. Linear parameter-varying control of systems of high complexity // Technische Universität Hamburg-Harburg. 2016. 402 p.
13. Shin J.Y. Quasi-linear parameter varying representation of general aircraft dy-namics over non-trim region // National Institute of Aerospace. 2007. 32 p.
14. Cisneros P.S.G., Voss S., Werner H. Efficient nonlinear model predictive con-trol via quasi-lpv representation // 2016 IEEE 55th Conference on Decision and Control (CDC). 2016. pp. 3216–3221.
15. Marcos A., Balas G.J. Development of linear-parameter-varying models for aircraft // Journal of Guidance, Control, and Dynamics. 2004. vol. 27. no. 2. pp. 218–228.
16. Kouvaritakis B., Cannon M. Nonlinear predictive control: theory and practice. 2001.
17. Allgöwer F., Zheng A. Nonlinear Model Predictive Control // Birkhäuser. 2000. 472 p.
18. Cisneros P.S.G., Werner H. Stabilizing model predictive control for nonlinear systems in input-output quasi-LPV form // 2019 American Control Conference (ACC). 2019. pp. 1002–1007.
19. Abbas H.S., Hanema J., Tóth R., Mohammadpour J., Meskin N. An improved robust model predictive control for linear parameter-varying input-output models // International Journal of Robust and Nonlinear Control. 2018. vol. 28(3). pp. 859–880.

20. Cisneros P.S.G., Voss S., Werner H. Efficient nonlinear model predictive con-trol via quasi-LPV representation // 2016 IEEE 55th Conference on Decision and Control (CDC). 2016. pp. 3216–3221.
21. Abbas H.S. et al. A robust MPC for input-output LPV models // IEEE Transac-tions on Automatic Control. 2016. vol. 61. no. 12. pp. 4183–4188.
22. Hanema J., Tóth R., Lazar M. Stabilizing non-linear MPC using linear parame-tervarying representations // 2017 IEEE 56th Annual Conference on Decision and Control (CDC). 2017. pp. 3582–3587.
23. Camacho E.F., Alba C.B. Model predictive control // Springer Science & Busi-ness Media. 2013. 405 p.
24. Maciejowski J.M. Predictive control: with constraints // Pearson education. 2002. 353 p.
25. Rossiter J.A. Model-based predictive control: a practical approach // CRC press. 2017. 344 p.
26. Rawlings J.B., Mayne D.Q. Model Predictive Control: Theory and Design // Nob Hill Publishing. 2010. 544 p.
27. Bemporad A., Ricker N.L., Morari M. Model Predictive Control Toolbox User's Guide // The MathWorks. 2019. 37 p.
28. Al-Hemeary N., Szederkényi G. Power regulation and linearization-based control design of a small satellite // 2019 12th International Conference on Develop-ments in eSystems Engineering 2019. pp. 646–650.
29. Fortescue P., Swinerd G., Stark J. Spacecraft systems engineering // John Wiley & Sons. 2011. 724 p.
30. Różowicz S., Zawadzki A. Input-output transformation using the feedback of nonlinear electrical circuits: Algorithms and linearization examples // Mathe-matical Problems in Engineering. 2018. vol. 2018. 13 p.
31. Cheng D., Isidori A., Respondek W., Tarn T.J. Exact linearization of nonlinear systems with outputs // Mathematical systems theory. 1988. vol. 21(1). pp. 63–83.
32. Zheng A. Some practical issues and possible solutions for nonlinear model predictive control // Nonlinear Model Predictive Control. 2000. pp. 129–143.
33. Polcz P. Optimal solar panel area computation for a CubeSat system using an offline MPC design. GitHub repository. 2020 URL: https://github.com/ppolcz/CubeSat_optimal_sparea (дата обращения: 02.03.2020).